American Mineralogist, Volume 83, pages 1246–1255, 1998

Thermal chemistry of H_2S and H_2O on the (100) plane of pyrite: Unique reactivity of defect sites

JEFFREY M. GUEVREMONT,[1] **DANIEL R. STRONGIN,**[1,*] **and MARTIN A.A. SCHOONEN**[2]

[1]Department of Chemistry, Temple University, Philadelphia, Pennsylvania 19122, U.S.A.
[2]Department of Earth and Space Sciences, State University of New York, Stony Brook, New York 11974-2100, U.S.A.

ABSTRACT

The interaction of a natural face of FeS_2 (100), cleaned in ultra-high vacuum (UHV), with H_2O and H_2S has been investigated with X-ray photoelectron spectroscopy (XPS), temperature programmed desorption (TPD), and the photoemission of adsorbed xenon (PAX). PAX is sensitive to the short-range order of the surface and allows the effects of defects on the surface reactivity of FeS_2(100) to be studied. PAX results suggest that both H_2S and H_2O bind most strongly to defect sites that we propose are, at least in part, sulfur anion vacancy sites. Whereas the majority of H_2O adsorbate desorbs from these sites in the temperature interval of 200–300 K, H_2S dissociates upon heating to 500 K into adsorbed surface hydrogen, S, and SH. This dissociation occurs on defect sites that then release part of the dissociation fragment, which is thought to be surface hydrogen, onto other regions of the pyrite surface that are proposed to be stoichiometric FeS_2. Heating to 600 K causes further reaction of S containing dissociation fragments with sulfur-deficient sites to form new surface sites that resemble FeS_2. The results also suggest that surface hydrogen dissolves into the pyrite bulk upon heating to 600 K.

INTRODUCTION

Pyrite is the most abundant metal sulfide on Earth and it forms in reducing environments, such as marine sediments, crater lakes, aquifers, water-logged soils, and in exhalative marine hydrothermal systems (Rickard and Luther 1995). Interaction between HS and iron sulfide mineral surfaces is of importance in the formation of pyrite. As shown recently (Rickard 1997; Rickard and Luther 1997), pyrite can be formed from aqueous systems consisting of iron monosulfides (amorphous FeS, mackinawite, or pyrrhotite) and dissolved HS. Once pyrite is formed via sulfidation of iron monosulfides, it can grow directly from solution leading to macroscopic, euhedral crystals (Schoonen and Barnes 1991). Growth of pyrite in solutions with HS as the sole sulfur source must involve a surface reaction in which adsorbed HS is transformed into a lattice-bound disulfide.

The H_2S-FeS_2 interaction is also of importance in systems where pyrite is not growing. Water in reducing environments often contain sulfidic sulfur, S^{2-}, in the form of H_2S, HS^-, or S^{2-} complexes (note S^{2-} species are not important in natural solutions, see Schoonen and Barnes 1988). A recent electrophoresis study (Bebie et al. 1997) showed that H_2S and HS^- are potential-determining ions on the pyrite surface. The addition of S^{2-} species renders the pyrite surface a negative charge over the entire pH range that can be evaluated using electrophoresis ($2<pH<11$). A similar effect was observed by Dekkers and Schoonen (1994) in their electrokinetic study of synthetic pyrrhotite and greigite. An analysis of all this prior research suggests that the interaction between H_2S and iron sulfides involves more than simply displacing >OH functional groups that are thought to be present on surface metal atoms. It is important to understand the interactions between H_2S and pyrite because this may influence the interaction of inorganic aqueous species (Kornicker and Morse 1991; Schoonen et al. 1992), organic aqueous species (Bebie and Schoonen 1997), and bacteria with the pyrite surface (Caldwell et al. 1984).

The H_2S-FeS_2 interaction is also of importance in the field of mineral separation and in the development of solar energy cells. Mineral separation via flotation is based on differences in hydrophobicity of mineral surfaces. The hydrophobicity of a mineral surface is routinely manipulated by addition of surfactant and other reagents to the ore slurry. As shown by Kydros et al. (1994) the flotation of pyrite can be manipulated by addition of Na_2S to the ore slurry. While the H_2S-FeS_2 interaction is of importance in applications such as desulfurization of coal and concentration of auriferous pyrite, there is no insight into the surface reactions that control the hydrophobicity of a pyrite surface in a Na_2S solution. Addition of Na_2S to pyrite in photocells appears to stabilize the pyrite (Chen et al. 1991). In the absence of Na_2S, illumination of pyrite leads to photocorrosion and loss of energy yield. Because the addition of Na_2S may significantly prolong the usefulness of pyrite in solar energy cells it is important to understand the H_2S-FeS_2 interaction (Bard 1982).

---

* E-mail: dstrongi@nimbus.ocis.temple.edu

0003–004X/98/1112–1246$05.00

This paper investigates the reaction of H_2S on pyrite in the ultra-high vacuum environment with emphasis on the effect of short-range order of the pyrite surface on this reaction. We also present results for the thermal chemistry of H_2O on $FeS_2(100)$ and contrast the reactivity of this adsorbate to that of H_2S. For both systems, the photoemission of adsorbed xenon (PAX) technique (Jablonski and Wandelt 1991; Wandelt et al. 1981) is used to characterize the short-range order of pyrite with and without adsorbate.

Due to the relatively weak interaction between Xe and the substrate, the binding energy (relative to the Fermi level) of the photoelectrons from adsorbed Xe depend on the electrostatic potential or work function of its adsorption site (Jablonski and Wandelt 1991; Wandelt et al. 1981). The local work function differs from the macroscopic work function; the latter is basically the average work function for the whole substrate, whereas the former is characteristic of microscopic regions of the sample. Hence, Xe atoms bound at different sites with non-equivalent electrostatic potentials can be distinguished during photoemission (given that the energy resolution of the spectroscopic technique is sufficient). Recent studies in our laboratory have shown that PAX is sensitive to the short-range order of $FeS_2(100)$. We emphasize two points concerning the interpretation of our PAX results here.

(1) Xe adsorption is inhibited by the presence of coadsorbates such as H_2O and H_2S on pyrite. The size of Xe (~4 Å diameter) prohibits a 1:1 correspondence between the amount of Xe inhibited and the surface coverage of H_2O and H_2S adsorbate.

(2) The presence of H_2O and H_2S changes the macroscopic work function of the sample. The binding energy of adsorbed Xe determined during photoemission, however, is not significantly (~0.2 eV) affected by this electronic perturbation. This experimental observation emphasizes the sensitivity of Xe to the local electrostatic potential of its adsorption site.

These points can only be considered assumptions at this juncture, but results presented in this contribution will support their validity. Based in large part on these assumptions, we show in this contribution that adsorbed H_2S and H_2O bind preferentially on defects, thought to be primarily sulfur-deficient sites on pyrite. H_2O is shown largely to simply thermally desorb from these defects by a temperature of 300 K. H_2S is shown to exhibit a more complex chemistry that involves dissociation on the defect sites and the migration of its dissociation fragments onto the less reactive stoichiometric FeS_2 surface.

EXPERIMENTAL METHODS AND TECHNIQUES

All experiments presented were performed in a bakeable stainless-steel ultra-high vacuum (UHV) chamber with a working base pressure of 3×10^{-10} Torr. UHV was obtained by ion, titanium sublimation, and turbomolecular pumps. The chamber was equipped with a quadrupole mass spectrometer, low energy electron diffraction (LEED) optics, double pass cylindrical mirror analyzer (CMA) with an electron gun for Auger electron spectroscopy (AES), X-ray source for X-ray photoelectron spectroscopy (XPS), and ion gun for sample cleaning.

A 6 cm^3 pyrite cube (single crystal) obtained from Longrono, Spain (Wards) was cut into a 2 mm thick square plate with an area of 1 cm^2. One side of the plate was an as grown surface, and any mechanical or chemical alteration of this natural surface was avoided outside of the UHV chamber. Laue-back reflection of the sample before its introduction into the UHV chamber showed sharp diffraction spots, and their symmetry indicated that the as-grown face was the (100) face, but the surface was visually striated.

For PAX, the pyrite plate was mounted on a tantalum foil with a conductive ceramic cement (Ag was a component) that increased thermal contact for enhanced cooling. For temperature programmed desorption (TPD) experiments no cement was used to allow sufficiently fast heating rates. In either case, the sample assembly was held in contact with a liquid nitrogen cryostat using tantalum wires spot-welded to the foil and mechanically clamped (electrically isolated) to the cryostat. Cooling down to temperatures in the range 78–80 K was routinely achieved by pumping on the liquid nitrogen within the cryostat. Heating of the sample was done resistively by passing current through the support wires via a copper braid that was held in intimate contact with the cold cryostat to reduce heat leaks through the copper heating wire. The temperature of the crystal was monitored with a type-K thermocouple, attached directly to the top edge of the sample using ceramic cement.

Preparation of an atomically clean $FeS_2(100)$ sample for UHV studies was carried out as described in detail by Chaturvedi et al. (1996). Briefly, the surface is prepared by using a cleaning cycle composed of 20 min 200 eV He^+ ion bombardment and 1 min anneals to 300 °C. Typically about 3–4 of these cycles were needed to reduce carbon and oxygen contamination below the detectable limit of AES. However, O 1s XPS did show some oxygen contamination suggesting that this contaminant resided beneath the outermost surface.

Both H_2O and H_2S were admitted into the UHV chamber through vacuum compatible leak valves. Exposures of these gases are quoted in Langmuirs ($1 \text{ L} = 10^{-6}$ Torr·s). H_2 was admitted into the UHV chamber through a ⅛″ stainless steel dosing-tube attached to a second UHV compatible variable leak valve. Dosing with atomic hydrogen was accomplished by moving the sample to within 2 cm of the end of the dosing tube. In between the sample and dosing tube was a tungsten filament that could be resistively heated so that it became white-hot. An undetermined fraction of H_2 (background pressure of 1×10^{-5} torr) passing over the white-hot filament produced H atoms, and a fraction of these subsequently interacted with the pyrite sample.

Some information concerning the desorption of particular products resulting from the thermal surface chemistry of H_2O and H_2S is inferred from temperature programmed desorption (TPD) experiments. TPD is a technique by which gaseous products can be detected and chemically identified, and in some cases the kinetics of surface reactions that lead to those products can be obtained. The typical TPD experiment involves adsorbing the molecule of interest at a temperature where dissociative chemisorption is prevented (this circumstance of course can not always be obtained). The sample temperature is then increased as a linear function of time. In the limit of infinite pumping speed in an UHV chamber, the mass spectrometer signal is proportional to the desorption rate of a particular product. In general, by analyzing the temperature at which a product shows a maximum desorption rate (known as T_P) and recording this for a variety of initial adsorbate coverages, estimates of the reaction order can be obtained. Also, by analyzing T_P as a function of heating rate and/or coverage in some cases, estimates of the activation energy of desorption can be obtained (see the seminal paper by Redhead 1962).

For a 1st order desorption process (T_P independent of coverage), we estimate the activation energy for desorption, E_a, from T_P (Eq. 1; Redhead 1962)

$$\frac{E_a}{RT_P^2} = \frac{\nu}{\beta}\exp\left(-\frac{E_a}{RT_P}\right) \qquad (1)$$

where R is the gas constant (cal-K^{-1}-mol^{-1}, β is the heating rate (K/s), and ν is the preexponential factor (s^{-1}). Because many surface adsorption processes are unactivated, E_a is taken in some situations to be close in value to the adsorption energy of the adsorbate.

TPD experiments presented in this contribution were performed with a heating rate of 8 K/s^{-1}. All desorbing species were monitored simultaneously by a multiplexed mass spectrometer. During a single experiment, for example, up to 9 ions could be monitored as a function of temperature. This allows products to be identified by comparing the mass spectrometer fragmentation pattern of desorbing species against reference gases (in this case H_2O and H_2S). The ionization region of the mass spectrometer was housed in an enclosure with a small aperture. During TPD experiments, the sample was translated to within 0.5 cm of the aperture hole, limiting the detection of gases desorbing from the sample supports.

XPS was performed by using unmonochromatized Mg*K*α radiation (1253.6 eV) as the excitation source. XPS measurements of the Xe $3d_{5/2}$ (for PAX) and O 1s levels were obtained with a CMA pass energy of 50 and 25 eV, respectively. All XPS binding energies presented in this paper are calibrated by aligning the Fe $2p_{3/2}$ core level of pyrite to 707.0 eV.

PAX data presented in this contribution were typically obtained at a sample temperature of 79–80 K and a Xe background pressure of 1 × 10^{-5} Torr (uncorrected for the ionization efficiency of Xe). This background pressure of Xe was needed to maintain a steady-state coverage of Xe on the sample (condensation temperature of Xe is ~60 K).

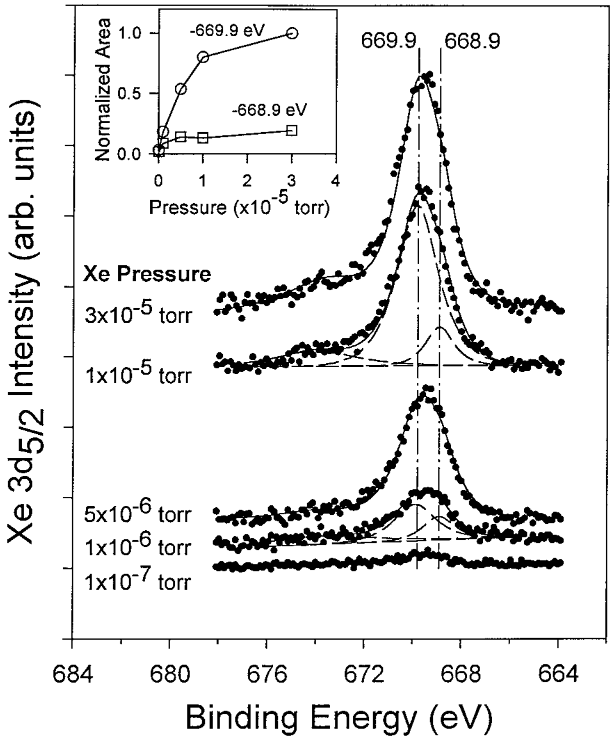

FIGURE 1. PAX data for atomically clean $FeS_2(100)$ as a function of the Xe background pressure. These data were obtained at a sample temperature of 79 K. The 669.9 and 668.9 eV features are thought to be associated with Xe adsorbed on stoichiometric and defect surface, respectively. The inset plots the area of these two PAX features as a function of Xe pressure.

RESULTS

PAX of clean $FeS_2(100)$

The Xe $3d_{5/2}$ signal intensity increased with pressure due to the increasing steady-state concentration of surface Xe (Fig. 1). Prior detailed studies in our laboratory concluded that two different types of sites adsorbed Xe on $FeS_2(100)$ and their relative contribution to the Xe $3d_{5/2}$ signal depended on the Xe background pressure (Guevremont et al. 1997). Those studies showed that Xe adsorbing on stoichiometric surface (i.e., FeS_2) and defect sites (thought to be anion vacancies and steps, etc.) result in Xe $3d_{5/2}$ binding energy features at ~669.9 and −668.9 eV, respectively. Stoichiometric surface refers here to regions of pyrite that have FeS_2 stoichiometry, such as terrace sites. The basis for both these binding energy peak assignments is presented elsewhere (Guevremont et al. 1997), but data presented below for H_2S and $H_2O/FeS_2(100)$ independently support these assignments. Specifically, we show below that these two Xe species that contribute to the Xe $3d_{5/2}$ signal can be isolated by coabsorbing Xe with H_2O or H_2S. There is a higher binding energy feature with a peak maximum near 674 eV that is needed to fit the 1 × 10^{-5} and 3 × 10^{-5} torr spectra. This feature appeared at high pressure and due to its high bind-

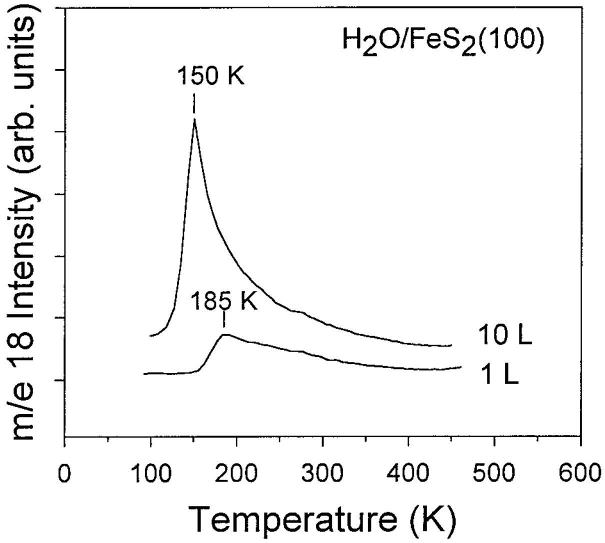

FIGURE 2. TPD of $H_2O/FeS_2(100)$ at 1 and 10 Langmuirs (L). The broad desorption tail in the temperature range of 200–300 K is thought to be due to H_2O desorption from defect sites.

ing energy we believe that it was due to a final state relaxation process that occurred in the Xe overlayer at high concentration as has been proposed elsewhere (Malafsky et al. 1992).

The inset to Figure 1 shows the relative contributions of the two peaks that are associated with stoichiometric and defect surface. The 668.9 eV peak area reached a plateau in the low 10^{-5} torr Xe range, but the 669.9 eV peak area continued to increase in this same range. We suggest on the basis of this latter result that even at a Xe pressure of 3×10^{-5} torr and a sample temperature of 79 K that the stoichiometric surface had not become saturated with Xe. Experimental difficulties prevented PAX data from being obtained at higher background pressures of Xe.

Thermal chemistry of H_2O on $FeS_2(100)$

TPD and XPS of $H_2O/FeS_2(100)$. The only desorbing species experimentally observed with the mass spectrometer during $H_2O/FeS_2(100)$-TPD was H_2O (Fig. 2). At the lower exposure of 1 L, the H_2O desorption trace exhibited a peak temperature, T_P, of 185 K, as well as broad desorption between this peak temperature and 300 K. It was suspected that this broad desorption temperature range is due to H_2O desorption from different sites with a range of activation energy of desorption values. We experimentally observed a significant decrease in T_P after $FeS_2(100)$ was exposed to 10 L of H_2O. A T_P of 150 K is typical of H_2O desorption from the multilayer (Thiel and Madey 1987; Gleason and Strongin 1995), and we infer from this result that multilayer or significant clustering of H_2O had occurred after such a high exposure.

Using Equation 1 we can estimate the difference in activation energy for desorption for H_2O bound on the stoichiometric ($T_P \approx 185$ K) and defect surface ($T_P \approx 250$ K) to be 10 and 15 kcal/mol^{-1}, respectively (preexponential factor of 10^{13} s^{-1} is assumed. If we assume that the adsorption of H_2O is unactivated these values can also be taken to be estimates of the relative adsorption energies of H_2O at the different sites.

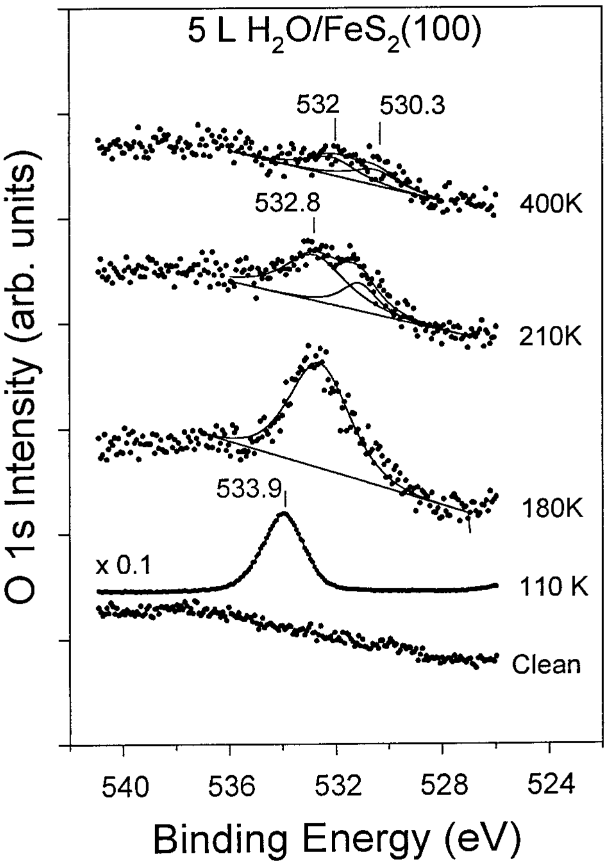

FIGURE 3. XPS O 1s data for $H_2O/FeS_2(100)$. Data were obtained by condensing a H_2O multilayer on $FeS_2(100)$ and then heating momentarily to the indicated temperature.

XPS-O 1s data (Fig. 3) were obtained by exposing $FeS_2(100)$ to 10 L of H_2O at 110 K and then individually heating the sample momentarily to 180, 200, and 400 K. The heating was done sequentially and after each heating step the sample was cooled back down to 110 K where data was obtained.

After a 10 L dose of H_2O, the O 1s peak was centered at 533.9 eV, a value that we associated with H_2O bound in a multilayer. Heating to 180 K led to a significant decrease in the O 1s intensity, consistent with TPD of $H_2O/FeS_2(100)$ (Fig. 2) that showed that the majority of H_2O desorbed after heating to 180 K. We suspect that the H_2O left on the surface after heating to 180 K was primarily bound intimately to $FeS_2(100)$, but the data did not rule out hydrogen bonded clusters. The shift of the O 1s binding energy from 533.9 to 532.8 eV upon heating from 110 to 180 K was consistent with the loss of the multilayer and the presence of a H_2O monolayer. Further heating to 200 K led to a decrease in the 532.8 eV feature and the appearance of a feature at 531 eV. The latter feature may have been present in the 180 K spectrum. We assigned this feature to a decomposition fragment of H_2O, either OH or atomic O. The former feature at 532.8 eV was assigned to H_2O that was bound on $FeS_2(100)$, because upon heating to 400 K this feature was eliminated, consistent with TPD that showed that H_2O entirely desorbed by 400 K. The 530.3 eV feature in the 400 K spectrum was probably due to an iron oxide because of its low binding energy value (Furuyama et al. 1978). The clean O 1s spectrum exhibited a smaller spectral feature near 530 that was believed to be strongly bound residual oxygen that could not be removed by our cleaning procedure. The 532 eV feature may have been due to hydroxyl (Nesbitt and Muir 1994; Knipe et al. 1995) or oxygen, but could not be definitively assigned in this study. However, based on integrated peak areas from the 180 and 400 K data we can state that 5% of the initial H_2O that adsorbed at 180 K dissociated upon heating to 400 K.

PAX of $H_2O/FeS_2(100)$. PAX data for $H_2O/FeS_2(100)$ were obtained after exposing pyrite to 10 L of H_2O at 79 K, and after heating this surface in a step-wise manner to 200 and 400 K. After each heating step the sample was cooled to 79 K where a Xe background pressure of 1×10^{-5} torr was admitted into the experimental chamber. An exposure of 10 L resulted in a H_2O multilayer on $FeS_2(100)$ and consistent with this contention was that the 80 K PAX spectrum showed almost no Xe $3d_{5/2}$ spectral weight (Fig. 4a). This result supported assumption 1 made in the Introduction. Heating to 200 K resulted in a PAX spectrum that showed significant Xe adsorption, suggesting that this thermal treatment left vacant sites on $FeS_2(100)$ where Xe could adsorb. Of note was that the peak maximum of the 200 K spectrum was near 670 eV, close to what has previously been associated with Xe adsorption on stoichiometric pyrite surface. Heating to 400 K resulted in a PAX spectrum that was similar to the clean spectrum indicating that the vast majority of adsorbate resulting from H_2O exposure at 80 K left the $FeS_2(100)$ surface.

Difference spectra (Fig. 4b) obtained by individually subtracting the 200 and 400 K data from the clean $FeS_2(100)$ data showed the Xe spectral weight that was lost (relative to the clean spectrum) upon heating $H_2O/FeS_2(100)$ to these temperatures. The 200 K difference spectrum showed a peak with a maximum at 669 eV, similar to the position that has been associated with defect sites on $FeS_2(100)$. Conversely, the 200 K spectrum of Figure 4a lost Xe intensity due to the blocking of defect sites by adsorbed H_2O (or its dissociation fragments) at 200 K. Although the 400 K PAX difference spectrum did not show clear evidence that defect sites (~669 eV) were blocked, we nevertheless inferred from the XPS data evidence that some defect sites were occupied by H_2O dissociation fragments.

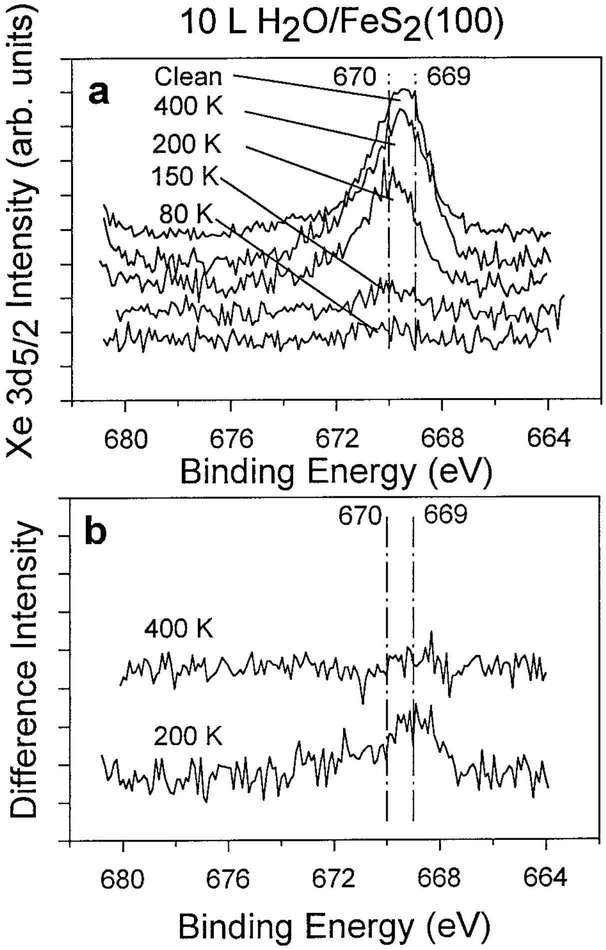

FIGURE 4. (**a**) PAX data obtained after $FeS_2(100)$ was exposed to 15 L of H_2O and then heated in stepwise fashion to the indicated temperatures. (**b**) Difference spectra obtained by individually subtracting the different temperature spectra from the clean surface spectrum.

Thermal chemistry of H_2S on $FeS_2(100)$

TPD of $H_2S/FeS_2(100)$. Figure 5 exhibits desorption traces for 10 L-H_2S/FeS_2 (adsorption was carried out at 110 K). The T_P of 180 K corresponds to an activation energy of desorption of ~10 kcal/mol (preexponential factor of 10^{13} s^{-1} is assumed). The possibility that H_2 evolution occurred during the thermal chemistry of H_2S was also investigated, but within experimental error little if any gaseous H_2 was experimentally observed.

PAX of $H_2S/FeS_2(100)$. After exposure of clean $FeS_2(100)$ to 15 L of H_2S at 79 K and subsequent annealing to the indicated temperatures, PAX data (obtained at a Xe pressure of 1×10^{-5} torr) showed a small Xe $3d_{5/2}$ feature (Fig. 6). The small amount of adsorbed Xe suggested that adsorbed H_2S blocked the majority of surface sites. Heating to 250 K resulted in the desorption of H_2S (as shown by TPD) and the associated 250 K-PAX spectrum showed a significant increase in Xe adsorption rel-

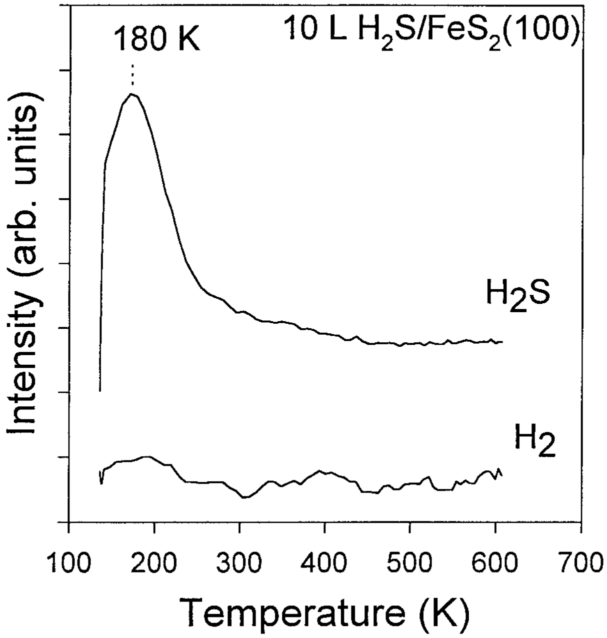

FIGURE 5. Thermal desorption traces of H_2S and H_2 for H_2S TPD. Adsorption of H_2S was carried out near 120 K.

ative to the 80 K spectrum. These PAX data showed that H_2S desorbed from the surface creating vacant surface sites on the pyrite surface that could adsorb Xe. Furthermore, after inspection of the 250 K difference spectrum (Fig. 6), which shows a peak at 669 eV, we propose that the H_2S resided on $FeS_2(100)$ at defect sites.

Heating of $H_2S/FeS_2(100)$ to 500 K led to an interesting experimental observation that had no parallel in our studies of $H_2O/FeS_2(100)$. Specifically, the amount of Xe that adsorbed on $FeS_2(100)$ decreased upon heating from 250 to 500 K, suggesting that the number of vacant sites decreased so that Xe adsorption was reduced. This decrease was due to the further filling of pyrite surface by the migration of surface bound H_2S or the dissociation fragments thereof. This contention was supported by the difference spectrum (inset of Fig. 6) obtained by subtracting the 500 K data from the clean surface data. The resulting spectrum showed enhanced spectral intensity and high binding energy spectral weight (in the region of ~670 eV) compared to the 250 K difference spectrum.

Further heating to 600 K resulted in increased Xe adsorption, relative to the 250 and 500 K spectrum. The 600 K difference spectrum (Fig. 6 inset) exhibited a "negative" feature peaked near −670 eV, indicating that heating to this temperature resulted in an increase of surface that adsorbed Xe in a similar way to stoichiometric FeS_2 surface. Also, of note was spectral weight near 668.9 eV that suggested that the defect concentration of the 600 K-surface was less than that of the clean surface.

TPD and PAX of $FeS_2(100)$ exposed to atomic hydrogen. Pyrite did not dissociate hydrogen as inferred from the experimental observation that no gaseous products were evolved during TPD after $FeS_2(100)$ was exposed to H_2. In contrast TPD after $FeS_2(100)$ was exposed to hydrogen atoms, generated by passing hydrogen over a white hot tungsten filament, exhibited gaseous H_2 and H_2S product with peak maxima at 400 and 430 K, respectively (Fig. 7).

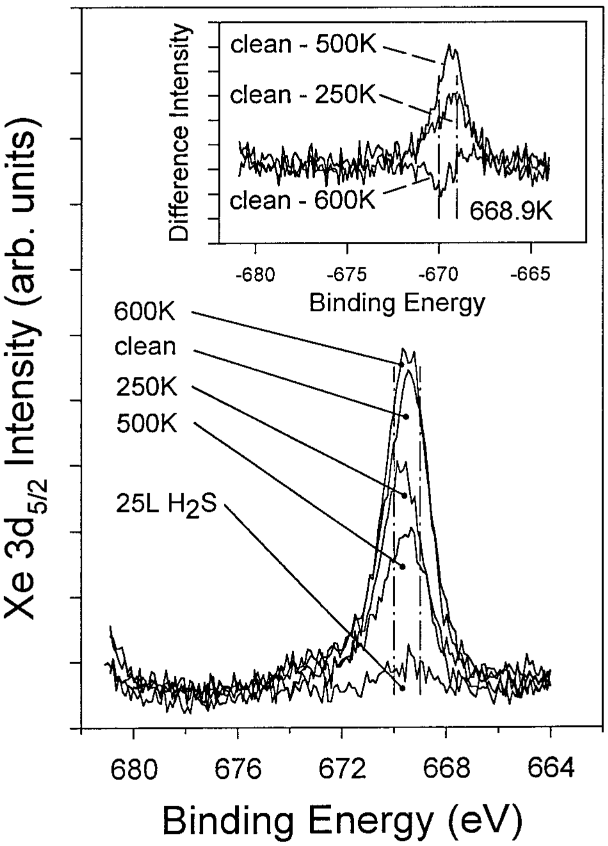

FIGURE 6. PAX data obtained after $FeS_2(100)$ was exposed to 15 L of H_2S and then heated in stepwise fashion to the indicated temperatures. Difference spectra shown in the inset were obtained by individually subtracting the different temperature spectra from the clean surface spectrum.

The PAX spectrum of $FeS_2(100)$ after this surface was exposed to H atoms at 80 K had a similar full-width-half-maximum as a clean surface spectrum (Fig. 8). The amount of Xe, however, that adsorbed to $H/FeS_2(100)$ was ~30% less than the amount of Xe that adsorbed to clean $FeS_2(100)$, suggesting that surface hydrogen was a site-blocker of Xe. Heating H/FeS_2 to 500 K led to a significant change in the spectrum. Most noticeable was the loss of spectral weight at high binding energy and a shift of the peak maximum to 669 eV, a position that has been previously associated with Xe adsorption on defect site. The difference spectrum obtained by subtracting the 500 K data from the 80 K spectrum, resulted in a feature peaked at ~670 eV and a "negative peak" near ~668.9 eV (inset to Fig. 8). The feature at 669.9 eV in the dif-

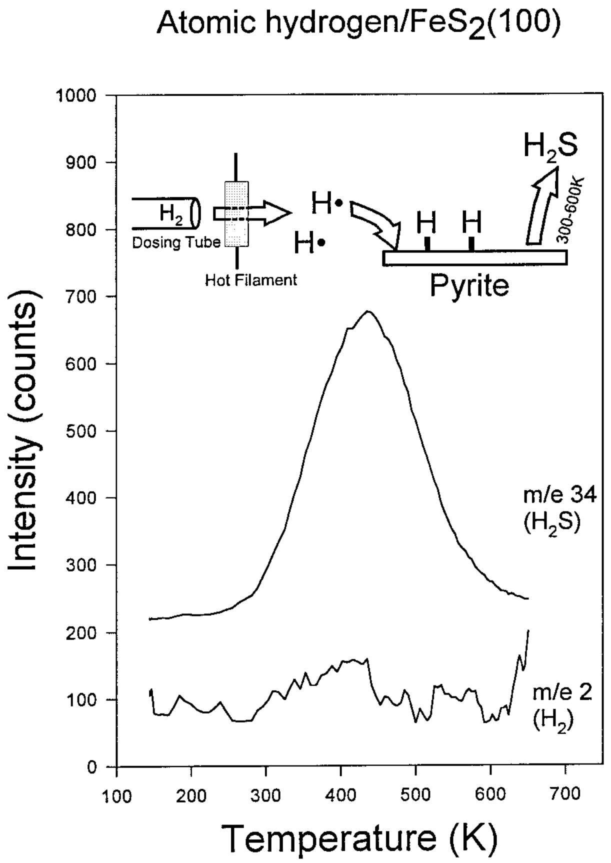

Figure 7. TPD results for $FeS_2(100)$ that was exposed to atomic H.

ference spectrum indicated that H_2S desorption, which was demonstrated by TPD (Fig. 7), resulted in a decrease in stoichiometric surface. Furthermore, on the basis of these PAX data we attributed the 420 K H_2S desorption peak to the reaction of surface hydrogen with lattice sulfur from stoichiometric surface. This reaction led to the creation of sulfur anion vacancies or defect site. (Repeated H atom TPD experiments degraded the crystal rapidly, causing a broadening of the TPD peaks.)

TPD of FeS_2 exposed to H_2S and atomic H (and D). $FeS_2(100)$ was exposed to 25 L of H_2S at 80 K, heated to 500 K to induce reaction, cooled back down to 80 K, and then exposed to atomic hydrogen. The objective of this pretreatment was to produce those fragments that inhibited Xe adsorption at 500 K and to determine their nature by extracting the fragment with atomic hydrogen into the gas phase during TPD. This H_2S pretreatment and exposure to H atoms at 80 K resulted in gaseous H_2 and H_2S evolution (Fig. 9a). In contrast to the experiments with no H_2S pretreatment (Fig. 7) a new H_2S desorption feature appeared near 270 K. This latter desorption feature was due to the addition of atomic hydrogen to surface fragments resulting from H_2S exposure at 80 K and heating to 500 K.

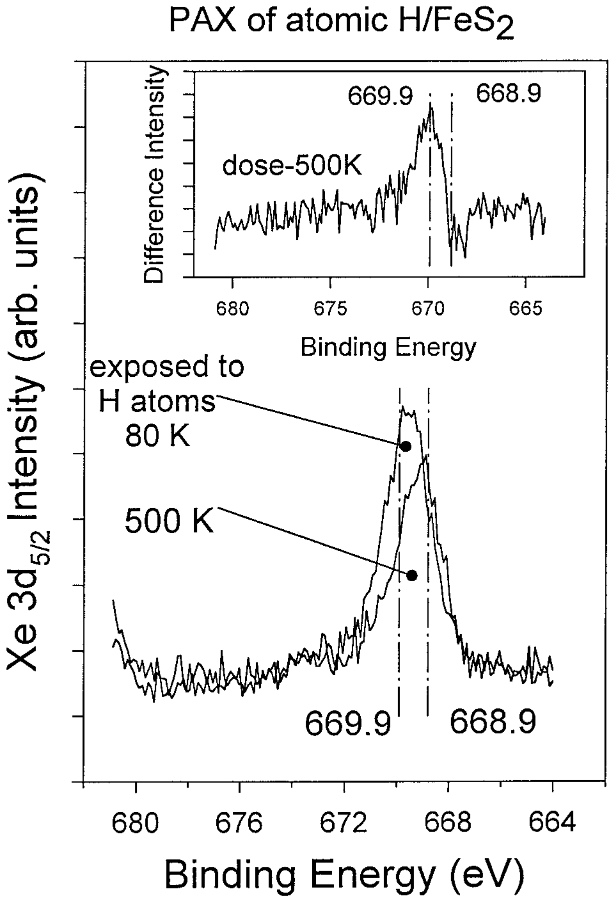

Figure 8. PAX data obtained after $FeS_2(100)$ was exposed to atomic H at 80 K and after heating to 500 K. The inset exhibits the difference of the 80 and 500 K spectrum and our interpretation of it is that upon heating to 500 K sulfur vacancy sites are created at the expense of stoichiometric surface.

Insight into the stoichiometry of the dissociation fragment was obtained through the use of atomic D, instead of H atoms. TPD data obtained by pretreating $FeS_2(100)$ with H_2S (as above) and then exposing the sample to atomic D showed D_2S, DHS, D_2, and HD evolution (Fig. 9b). D_2S evolution at 420 K was due to the abstraction of lattice S by D atoms. D_2S evolution at 270 K was presumably due to the reaction of D atoms with weakly bound atomic S resulting from the dissociation of H_2S. Last, DHS evolution at 270 K was due to the reaction of D atoms with S-H fragments resulting from H_2S dissociation. The larger DHS desorption feature with a peak temperature of 420 K was attributed to the reaction of surface H (supplied by H_2S dissociation) and D atoms with lattice S.

DISCUSSION

Thermal chemistry of H_2O on $FeS_2(100)$

At least in the vacuum environment, the results for H_2O and H_2S on $FeS_2(100)$ suggest two contrasting pictures of

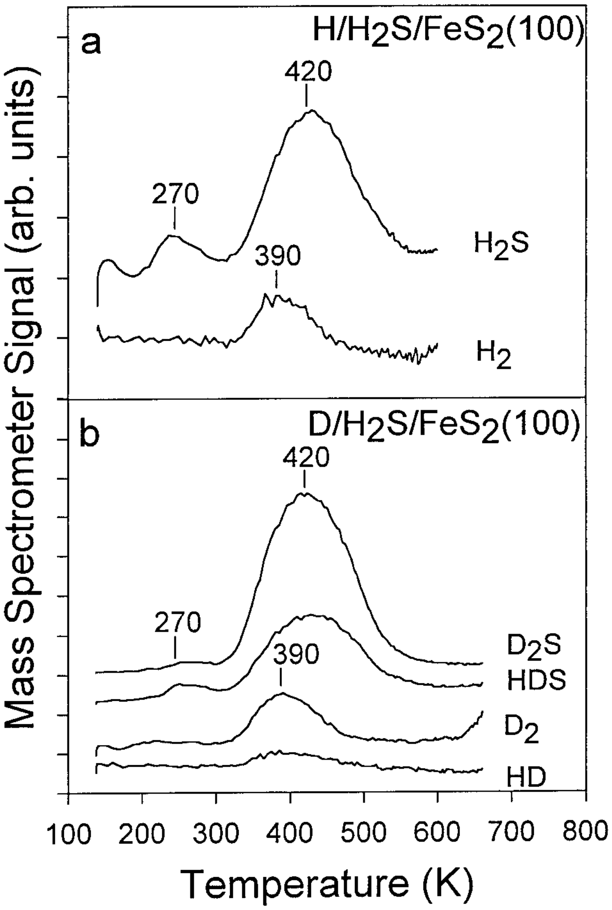

FIGURE 9. TPD results for $FeS_2(100)$ that was exposed to 25 L H_2S at 80 K, heated to 500 K, cooled back to 80 K and exposed to atomic (**a**) H and (**b**) D.

the surface. For H_2O, adsorption is strongest at defect sites that are tentatively assigned to be at least in part sulfur-vacancy sites. These defect sites almost certainly include step sites, which have been imaged with tunneling microscopy (Eggleston and Hochella 1992), and exhibit perturbations of electronic structure relative to terrace sites. We emphasize that in our experiments, once the $FeS_2(100)$ was atomically cleaned by our UHV-based He^+ bombardment method, the defect contribution, could not be increased by further He^+ bombardment time. Specifically, the ratio of the two Xe $3d_{5/2}$ features that characterize a particular clean $FeS_2(100)$ surface remained constant within experimental error after repeated He^+ cleaning cycles. Hence, the defects investigated here are intrinsic to the natural pyrite surface, and were not introduced on the surface by our cleaning procedure. Furthermore we estimate that the defect sites makeup about 14% of the $FeS_2(100)$ surface based on our results that show that at a Xe pressure of 3×10^{-5} torr the 669.9 eV (stoichiometric surface) to 668.9 eV (sulfur-vacancy) peak area ratio is ~6 (Fig. 1). This is only an estimate, because saturation may not of been achieved under our experimental conditions, and the amount of Xe that adsorbs on a given defect site need not be equal to the amount of Xe that adsorbs on a stoichiometric surface site (Malafsky 1994).

H_2O remains bound to defect sites up to 300 K. In contrast, H_2O bound to the stoichiometric surface of $FeS_2(100)$ is more weakly bound and desorbs from pyrite in vacuum at a temperature below 200 K. XPS suggests that 5% of the H_2O monolayer present at 180 K dissociates upon heating to 400 K and results in the formation of iron oxide, that on the basis of PAX is postulated to occur on defect sites. We do not find any experimental evidence for any H_2O dissociation fragments residing on the stoichiometric surface.

Thermal chemistry of H_2S on $FeS_2(100)$

H_2S initially adsorbed on $FeS_2(100)$ at 79 K, remains bound to defects, but vacates the stoichiometric surface of $FeS_2(100)$ upon heating to 250 K. This chemistry exhibited by H_2S is similar to that of H_2O in this temperature range. Beyond this temperature, however, the thermal chemistry of H_2S is dissimilar to that of H_2O. Whereas the majority of H_2O binding to defect sites at 200 K desorbs from pyrite upon heating to 300 K, H_2S (or its dissociation fragments) binding to defect sites at 200 K does not show desorption with subsequent heating to 600 K.

At least two experimental observations derived from PAX reveal some of the thermal chemistry details of H_2S. First, the PAX intensity decreases upon heating $H_2S/FeS_2(100)$ from 250 to 500 K, suggesting that the surface coverage of adsorbate increases upon heating to 500 K. It is proposed that H_2S dissociates in this interval resulting in the filling of surface sites that could otherwise adsorb Xe. TPD experiments suggest that these fragments consist of surface H, S, and SH. TPD results also suggest that at least a fraction of the S resulting from H_2S dissociation is chemically distinct from lattice S at a temperature of 500 K. This later statement is inferred from TPD experiments that show that S resulting from H_2S dissociation is removed by atomic hydrogen at a lower temperature than lattice S.

The second PAX observation is that the loss in PAX intensity upon heating $H_2S/FeS_2(100)$ from 250 to 500 K, at least partially occurs in a region of the PAX spectrum that has been attributed to Xe adsorption on stoichiometric surface. In other words, whereas H_2S appears to be exclusively binding to defect sites at 250 K, the dissociation products migrate on to the stoichiometric surface of $FeS_2(100)$.

We suspect that at least part of the decrease in Xe adsorption on the stoichiometric surface upon heating to 500 K is due to the reaction of surface H (resulting from H_2S dissociation) with lattice S, resulting in S-H that can block Xe adsorption. This contention would be consistent with TPD experiments that show that DHS product desorbs with a T_P of 420 K after $H_2S/Fe(100)$ is heated to 500 K and then exposed to atomic D at 80 K.

More ambiguity is present in determining the location of SH and S dissociation products. PAX of 500 K-H_2S/FeS_2(100) suggests that the majority of defect sites are covered, but upon heating to 600 K, some of the defect sites are vacated and new surface adsorption sites for Xe form. These new adsorption sites have an electrostatic potential similar to FeS_2. This result might suggest that sulfur-deficient defect sites become more like stoichiometric regions of pyrite via sulfur addition from H_2S dissociation. In other words, more stoichiometric surface is produced at the expense of defect surface.

There does, however, exist some uncertainty in this interpretation. Specifically, on the basis of PAX the gain in the number of stoichiometric surface sites appears greater than the loss in defect sites (Fig. 6, clean ~ 600 K difference spectrum). It may be, however, that this apparent contraction is simply due to a circumstance that has more Xe adsorbing on any given stoichiometric-like site than any given defect site. The abstraction of S from FeS_2 with atomic hydrogen as H_2S product, for example, leads to a larger decrease in Xe adsorption on stoichiometric surface than increase in Xe adsorption on defect sites (see Fig. 8). As stated above, prior research also has shown the difficulties in obtaining site concentrations through the use of PAX (Malafsky 1994).

On the basis of this interpretation we surmise that at least part of the H_2S dissociation product, SH and S, at 500 K are located on defect sites (Fig. 10). We cannot rule out, however, the possibility that these types of fragments also reside on the stoichiometric surface. Such a scenario would require that SH and S be removed from the stoichiometric surface upon heating to 600 K, based on PAX. Because no gaseous products are detected in the 500–600 K interval, diffusion of adsorbate into the pyrite would be the most likely pathway. Whether this occurs for S and SH fragments cannot be determined unambiguously from our data. Our data is more conclusive with regard to placing surface hydrogen on the stoichiometric surface at 500 K so the dissolution of this species presumably does occur upon heating to 600 K.

The experimental observation that the majority of defect sites on FeS_2(100) that are filled at 250 K became vacant after heating to 600 K suggests that, whereas a fraction of the S-deficient sites can be converted to more S-rich sites, another fraction intrinsically resists sulfur addition. In effect these more stable defect sites may facilitate or catalyze the dissociation of H_2S on the mineral surface so that the dissociation fragments can then undergo further thermal chemistry on less reactive stoichiometric mineral surface.

Relevance of UHV studies to real processes?

Because of the difference in environment between UHV employed in this study and the natural environment one must be careful in extending our UHV results to understand H_2S-pyrite reactions in the natural environment. Some of our results, however, appear quite relevant, and have intriguing implications for the understanding of real processes.

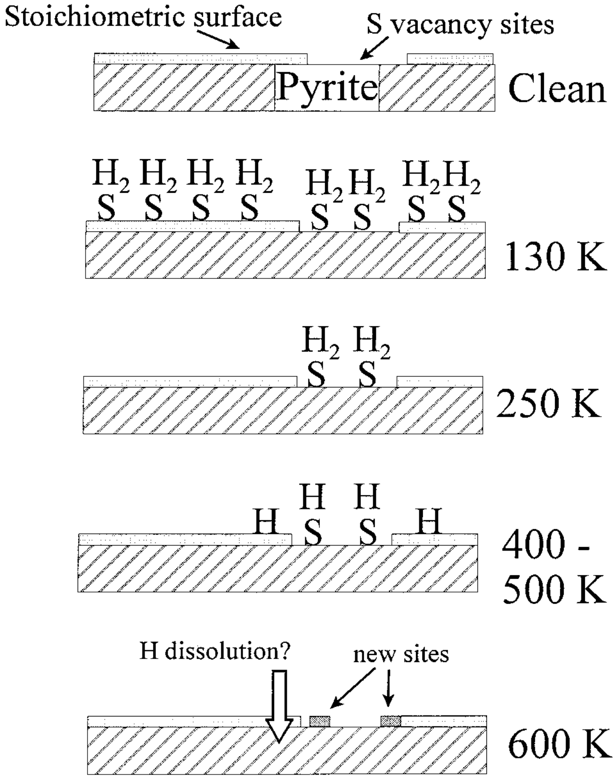

FIGURE 10. A proposed model for the thermal chemistry of H_2S on FeS_2(100). Adsorption of H_2S on FeS_2(100) at 100 K results in an adsorbed monolayer with H_2S binding on stoichiometric as well as defect sites. Heating to 250 K removes weakly bound H_2S from the stoichiometric surface. Heating to 500 K results in the migration of H_2S dissociation fragments on to stoichiometric surface. Whereas the diffusion of H is well-supported by our data, it cannot be determined unambiguously whether S containing species also migrate. Heating to 600 K results in the diffusion of surface hydrogen into the pyrite bulk and the formation of new surface sites from the addition of S (resulting from H_2S dissociation) to sulfur-vacancy sites.

The interaction of H_2S with pyrite in aqueous solution is important with regard to pyrite growth. For the growth of pyrite particles the dissociation of H_2S is a necessary step. Our results suggest that this step is facilitated by intrinsic structural imperfections on pyrite that can dissociate H_2S and release the fragments onto the growing crystal. Furthermore, our study suggests that in the vacuum environment surface hydrogen is the primary dissociation fragment that can diffuse from defect to the stoichiometric surface. Experimental results are less conclusive with regard to whether species containing S show this same thermally induced migratory behavior in vacuum. Such a mechanism, however, would provide a possible route through which the relatively unreactive stoichiometric pyrite surface can be constantly supplied with reactant for further growth.

Rickard and Luther (1997) proposed that the growth of pyrite via the interaction of FeS and H_2S in the aqueous environment involves the evolution of H_2. Based on our results, the reaction of surface hydrogen to form gaseous H_2 on the FeS_2 surface is not a facile process, because an insignificant amount of gaseous H_2 product is observed during the decomposition of H_2S in vacuum. This result might be taken to support the proposal by Rickard and Luther that H_2 evolution results from the direct interaction between the hydrogen in H_2S reactant (presumably not assisted by the surface). We also point out that the fate of hydrogen might be to incorporate into the pyrite lattice during the growth of pyrite.

Our results may also be relevant toward the goal of understanding the charge development behavior of pyrite in H_2S bearing solution. Electrophoresis studies conducted by Bebie et al. (1997) for H_2S/FeS_2 have determined that H_2S is a charge determining species in solution. Our results are consistent with this prior experimental observation, because they indicate that H_2S dissociates on $FeS_2(100)$ resulting in the deposition of S, SH, and surface H. Future experiments will involve investigating the nature of the surface groups with UHV based techniques, which are present on pyrite, subsequent to exposure to H_2S bearing solution.

ACKNOWLEDGMENTS

D.R.S. and M.A.A.S. greatly appreciate support from the Department of Energy, Basic Energy Sciences from grant DEFG0296ER14644 and DEFG029ER14633, respectively. All the authors also greatly appreciate the in-depth and thoughtful review of Carl Moses and an anonymous reviewer that significantly improved this contribution.

REFERENCES CITED

Bard, A.J. (1982) Design of semiconductor photoelectrochemical systems for solar energy conversion. Journal of Chemistry and Physics, 86, 172–177.

Bebie, J. and Schoonen, M.A.A. (1997) Interactions of phosphate and organics with pyrite (FeS_2) under anox-rayic conditions: implications for the origin of life. American Chemical Society-Northwest Regional Meeting.

Bebie, J., Schoonen, M.A.A., Fuhrmann, M., and Strongin, D.R. (1998) Surface charge development on transition metal sulphides: an electrokinetic study. Geochimica Cosmochimica Acta, 62, 633–642.

Caldwell, D.E., Kieft, T.L., and Brannan, D.K. (1984) Colonization of sulfide-oxygen interfaces on hot spring tufa by Thermothrix thiopara. Geomicrobiology Journal, 3, 181–200.

Chaturvedi, S., Katz, R., Guevremont, J., Schoonen, M.A.A., and Strongin, D.R. (1996) XPS and LEED study of a naturally occurring single crystal surface of pyrite. American Mineralogist, 81, 261–264.

Chen, G., J.Z., Fan, F., and Bard, A.J. (1991) Electrochemical investigation of the energetics of irradiated FeS_2 (pyrite) particles. Journal of Physics and Chemistry, 95, 3682–3687.

Dekkers, M.J. and Schoonen, M.A.A. (1994) An electrokinetic study of synthetic greigite and pyrrhotite. Geochimica Cosmochimica Acta, 58, 4147–4153.

Eggleston, C.M. and Hochella, M.F. (1992) Scanning tunneling microscopy of pyrite {100} surface structure and step reconstruction. American Mineralogist, 77, 221–224.

Furuyama, M., Kishi, K., and Ikeda, S. (1978) The adsorption of SO_2 on iron surfaces by X-ray photoelectron spectroscopy. Journal of Electron Spectroscopy and Related Phenomena, 13, 59–67.

Gleason, N.R., Chaturvedi, S., and Strongin, D.R. (1995) Interaction of Water with NiAl(110): A TPD, EELS, and XPS investigation. Surface Science, 326, 27–41.

Guevremont, J.M., Strongin, D.R., and Schoonen, M.A.A. (1997) Effects of surface imperfections on the binding of CH_3OH and H_2O on $FeS_2(100)$: using adsorbed Xe as a probe of mineral surface structure. Surface Science, 391(1–3), 109.

——— (1998) Photoemission of Adsorbed Xenon, X-ray Photoelectron Spectroscopy, and Temperature-Programmed Desorption Studies of H_2O on $FeS_2(100)$. Langmuir, 14(6), 1361–1366.

Jablonski, A. and Wandelt, K. (1991) Quantitative aspects of ultraviolet photoemission of adsorbed xenon-A review. Surface and Interface Analysis, 17, 611–627.

Knipe, S.W., Mycroft, J.R., Pratt, A.R., Nesbitt, H.W., and Bancroft, G.M. (1995) X-ray photoelectron spectroscopic study of water adsorption on iron sulphide minerals. Geochimica Cosmochimica Acta, 59, 1079–1090.

Kornicker, W.A. and Morse, J.W. (1991) Interactions of divalent cations with the surface of pyrite. Geochimica Cosmochimica Acta, 55, 2159–2171.

Kydros, K.A., Gallios, G.P., and Matis, K.A. (1994) Electrolytic Flotation of Pyrite. Journal of Chemical Technology and Biotechnology, 59, 223–232.

Malafsky, G.P. (1994) The effect of sputter temperature on vacancy island behavior on Ni(111) measured by photoemission of adsorbed xenon. Surface Science, 306, L539–L544.

Malafsky, G.P., Fu, S.S., and Hsu, D.S. (1992) Photoemission of adsorbed xenon study of surface defects generated by ion bombardment of nickel(111). Journal of Vacuum Science and Technology A, 10(6), 3472–3477.

Nesbitt, H.W. and Muir, I.J. (1994) X-ray photoelectron spectroscopic study of a pristine pyrite surface reacted with water vapor and air. Geochimica Cosmochimica Acta, 58(21), 4667–4679.

Redhead, P.A. (1962) Thermal desorption of gases. Vacuum, 12, 203.

Rickard, D. (1997) Kinetics of pyrite formation by the H2S oxidation of iron(II)monosulfide in aqueous solutions between 25 and 125 °C: The rate equation. Geochimica Cosmochimica Acta, 61(1), 115–134.

Rickard, D. and Luther, G.W. (1995). Chemistry of iron sulfides in sedimentary environments. In M.A. Vairavamurthy and M.A.A. Schoonen, Eds., Geochemical Transformations of Sedimentary Sulfur, p. 168–193. American Chemical Society Symposium Series 612, Washington, D.C.

——— (1997) Kinetics of pyrite formation by the H2S oxidation of iron(II)monosulfide in aqueous solutions between 25 and 125 °C: The mechanism. Geochimica Cosmochimica Acta, 61(1), 135–148.

Schoonen, M.A.A. and Barnes, H.L. (1988) An approximation of the second dissociation constant for H2S. Geochimica Cosmochimica Acta, 52, 649–654.

——— (1991) Mechanisms of pyrite and marcasite formation from solution I: Nucleation of FeS_2 below 100 °C. Geochimica Cosmochimica Acta, 55, 1495–1504.

Schoonen, M.A.A., Fisher, N.S., and Wente, M. (1992) Gold sorption onto pyrite and goethite: A radiotracer study. Geochimica Cosmochimica Acta, 56, 1801–1814.

Thiel, P.A. and Madey, T.E. (1987) The interaction of water with solid surfaces: fundamental aspects. Surface Science Reports, 7, 211.

Wandelt, K., Hulse, J., and Küppers, J. (1981) Site-selective adsorption of xenon on a stepped Ru(0001) surface. Surface Science, 104, 212–239.

MANUSCRIPT RECEIVED DECEMBER 3, 1997
MANUSCRIPT ACCEPTED JULY 9, 1998
PAPER HANDLED BY GLENN A. WAYCHUNAS